Supporting Information

Rational pore engineering reveals the relative contribution of enzymatic sites and self-assembly towards rapid ferroxidase activity and mineralization: Impact of electrostatic guiding and cage-confinement in bacterioferritin

Akankshika Parida[#], Gargee Bhattacharyya[#], Swagatika Mallik[#], Rabindra K. Behera[*]

Department of Chemistry, National Institute of Technology, Rourkela - 769008, Odisha, India.

# These authors contributed equally

*To whom correspondence should be addressed: Rabindra K. Behera, Tel: +91-661-2462980; Fax: +91-661-2462651; E-mail: beherarabi@nitrkl.ac.in

Table S1. Oligonucleotide primers designed for site-directed mutagenesis.

Mtb BfrA variants	Oligonucleotide primer (5′ to 3′)
E121A_For	CGGCAACGATTTT**CGC**CAGCAGTACGGCG
E121A_Rev	CGCCGTACTGCTG**GCG**AAAATCGTTGCCG
E121Q_For	GGCAACGATTTTC**TGC**AGCAGTACGGCGC
E121Q_Rev	GCGCCGTACTGCT**GCA**GAAAATCGTTGCC
E121K_For	CGGCAACGATTTTC**TTC**AGCAGTACGGCGCT
E121K_Rev	AGCGCCGTACTGCT**GAA**GAAAATCGTTGCCG
E121F_For	TCGTCGGCAACGATTTT**GAA**CAGCAGTACGGCGCTGG
E121F_Rev	CCAGCGCCGTACTGCTG**TTC**AAAATCGTTGCCGACGA

Changes in the nucleotide base pair positions are underlined and highlighted in bold.

Table S2: Overexpression conditions employed for assembly-defective 3-fold pore variants of *Mtb* BfrA (E121K and E121F).

Mtb BfrA Variant	Condition	IPTG (mM)	Incubation period after IPTG induction	rpm	Temperature after IPTG induction	Betaine (mM)	Sorbitol (mM)	Inference (Cage-assembly)
E121K	**1**	0.5	4 hrs	200	37°C	2.5	-	Partial
	2	0.5	4 hrs	200	37°C	2.5	660	Partial
	3	0.25	10 hrs	100	25°C	-	-	Partial
E121F	**4**	0.5	4 hrs	200	37°C	2.5	-	None
	5	0.5	4 hrs	200	37°C	2.5	660	None
	6	0.25	10 hrs	100	25°C	-	-	None
E121K & E121F	Routine protocol	0.5	4 hrs	200	37°C	-	-	None

Table S3. Average hydrodynamic diameters of apo- and iron biomineral encapsulated ferritin protein samples determined from dynamic light scattering (DLS) studies.

Ferritin	Hydrodynamic size (nm)		
	Apo-ferritin*	100 Fe/cage†	480 Fe/cage†
WT	12.6 ± 0.4	12.6 ± 0.9	13.5 ± 0.9
E121A	11.7 ± 1.1	11.7 ± 1.0	13.5 ± 1.0
E121Q	13.5 ± 1.9	13.5 ± 1.3	15.7 ± 1.3
E121K	5.6 ± 0.6	15.7 ± 1.6	50.7 ± 2.5
E121F	8.7 ± 0.8	16.9 ± 1.8	32.7 ± 3.6

*Apo-ferritin hydrodynamic sizes were obtained from **Fig. 2**.

†Hydrodynamic sizes for mineralized ferritins were determined from **Fig. S11**.

Table S4. Apparent kinetic parameters for the formation of $[Fe^{3+}\text{-}O]_x$ species (measured at 350 nm) by the *Mtb* BfrA variants, obtained by non-linear fitting to the Hill equation (see methods and Fig. S5).

Ferritin	Apparent Parameters				
	v_{max}*	k_{cat}† s^{-1}	K_m, M	k_{cat}/K_m, $M^{-1}\ s^{-1}$	Hill coefficient (n)
WT	0.19 ± 0.01	0.18 ± 0.01	14.9×10^{-6}	1×10^4	2.2 ± 0.3
E121A	0.18 ± 0.01	0.17 ± 0.01	19.4×10^{-6}	9×10^3	1.8 ± 0.4
E121Q	0.20 ± 0.02	0.20 ± 0.02	20.6×10^{-6}	1×10^4	1.7 ± 0.2
E121K	0.03 ± 0.01	0.03 ± 0.01	N.D.	N.D.	N.D.
E121F	0.12 ± 0.02	0.12 ± 0.02	30.5×10^{-6}	4×10^3	1.1 ± 0.1

*Apparent v_{max} ($\Delta A/\Delta t$, sec^{-1})

†Determined from the formula for turnover number: k_{cat} (apparent) = v_{max} (apparent)/$[E_T]$ where $[E_T]$ is the total enzyme (i.e BfrA cage) concentration. Here, $[E_T]$ is maintained as 1.04 μM for all the variants.

N.D. Not determined due to small change in absorbance.

Table S5. Thermodynamic parameters determined from the chemical and thermal unfolding of WT BfrA and its variants.

Mtb BfrA variants	GdnHCl denaturation†			Thermal denaturation†
	C_m (M)	ΔG_{Aq} (kJ/mol)	m (kJ/mol/M)	T_m (°C)
WT	7.4 ± 0.2*	21.8 ± 2.1*	2.9 ± 0.3*	90 ± 4*
E121A	7.0 ± 0.1	18.9 ± 1.9	2.6 ± 0.3	90 ± 2*
E121Q	7.0 ± 0.2	22.4 ± 2.4	3.1 ± 0.4	84 ± 2*
E121K	1.6 ± 0.1	8.1 ± 1.4	4.7 ± 0.6	78 ± 4
E121F	1.6 ± 0.1	7.2 ± 1.5	4.2 ± 0.5	80 ± 3

*The apparent thermodynamic parameters.

† Parameters for GdnHCl denaturation and thermal denaturation were obtained from **Fig. 6** and **Fig. S13** respectively.

Table S6: Comparison of the intra-subunit and inter-subunit distances measured from the separation of the 121 residue of respective ferritin variants with R109, E110 and K122 residues. Distance is calculated between the highlighted atoms.

Ferritin	Intra-subunit distances (A°)			Inter-subunit distances (A°)			
	122* – 121	121 – 109	121 –110	121 – 122*	121 – 121	121– 110	121 – 109
WT (Alpha fold)	9.6 (NH_2 – OH)	3.1 (OH – NH_2)	12.4 (OH – OH)	11.6 (OH – NH_2)	6.5 (OH – OH)	14.1 (OH – OH)	3.6 (OH – NH_2)
WT (3UOI)	10.1 (NH_2 – OH)	2.7 (OH – NH_2)	12.4 (OH – OH)	10.5 (OH – NH_2)	6.3 (OH – OH)	13.8 (OH – OH)	3.7 (OH – NH_2)
E121A	9.8 (NH_2 – H)	5.8 (H – NH_2)	15.6 (H – OH)	15.7 (H – NH_2)	10.7 (H – H)	17.5 (H – OH)	10.0 (H – NH_2)
E121Q	13.1 (NH_2 – NH_2)	3.2 (NH_2 – NH_2)	13.6 (NH_2 – OH)	17.2 (NH_2 –NH_2)	6.3 (NH_2 – NH_2)	16.2 (NH_2 – OH)	5.7 (NH_2 – NH_2)
E121K	14.5 (NH_2 – NH_2)	6.3 (NH_2 – NH_2)	13.2 (NH_2 – OH)	17.0 (NH_2 –NH_2)	4.0 (NH_2 – NH_2)	15.1 (NH_2 – OH)	8.0 (NH_2 – NH_2)
E121F	9.1 (NH_2 – C)	8.0 (C – NH_2)	18.9 (C – OH)	13.3 (C – NH_2)	10.1 (C – C)	21.5 (C – OH)	10.0 (C – NH_2)

*122 oriented towards the interior

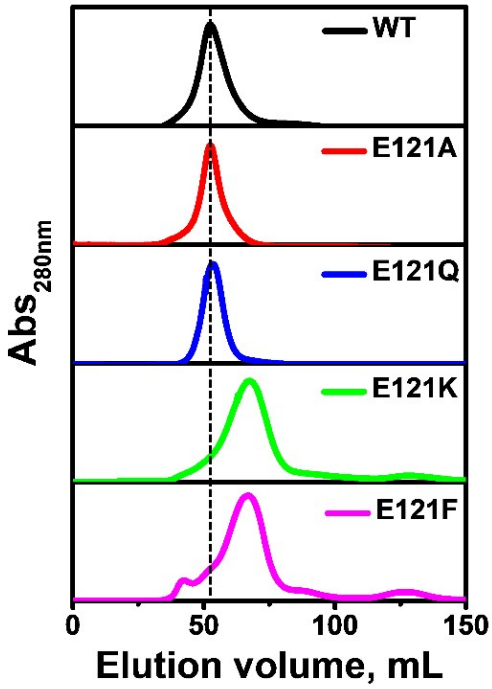

Figure S1. Elution profile (size exclusion chromatogram) of WT BfrA and its variants. The as-purified protein samples collected after IEC, were passed through Sephacryl S-300 HR column previously equilibrated with 20 mM Tris containing 100 mM NaCl (pH 8.0). The less intense bands observed at high elution volumes for E121K and E121F are possibly due to the presence of a small amount of nucleic acid (see **Methods**).

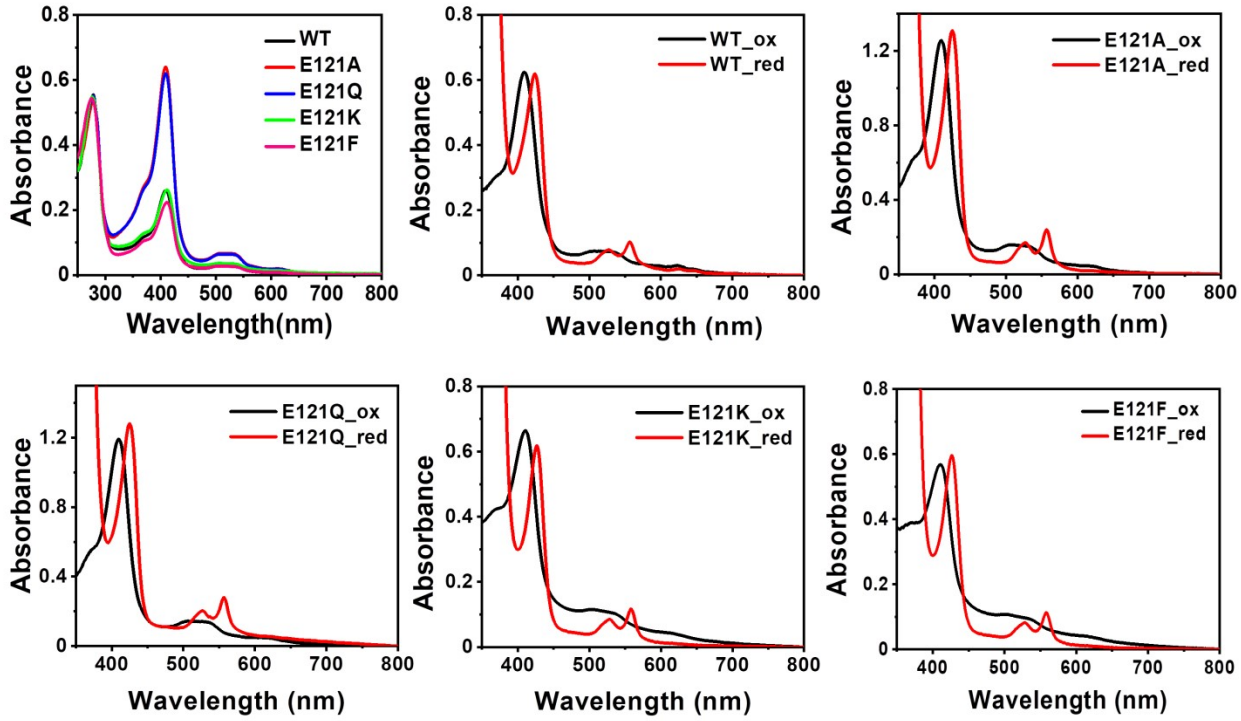

Figure S2. UV-visible absorption spectra of as-purified WT BfrA and its variants, in their oxidized and reduced form. The reduction process was initiated by the addition of 20 µL of 5 mM sodium dithionite to 2 µM cage or cage equivalent of protein samples (see **Methods**). The E121A and E121Q variants were found to bind more heme compared to the WT, E121K and E121F variants that exhibited a lower heme content.

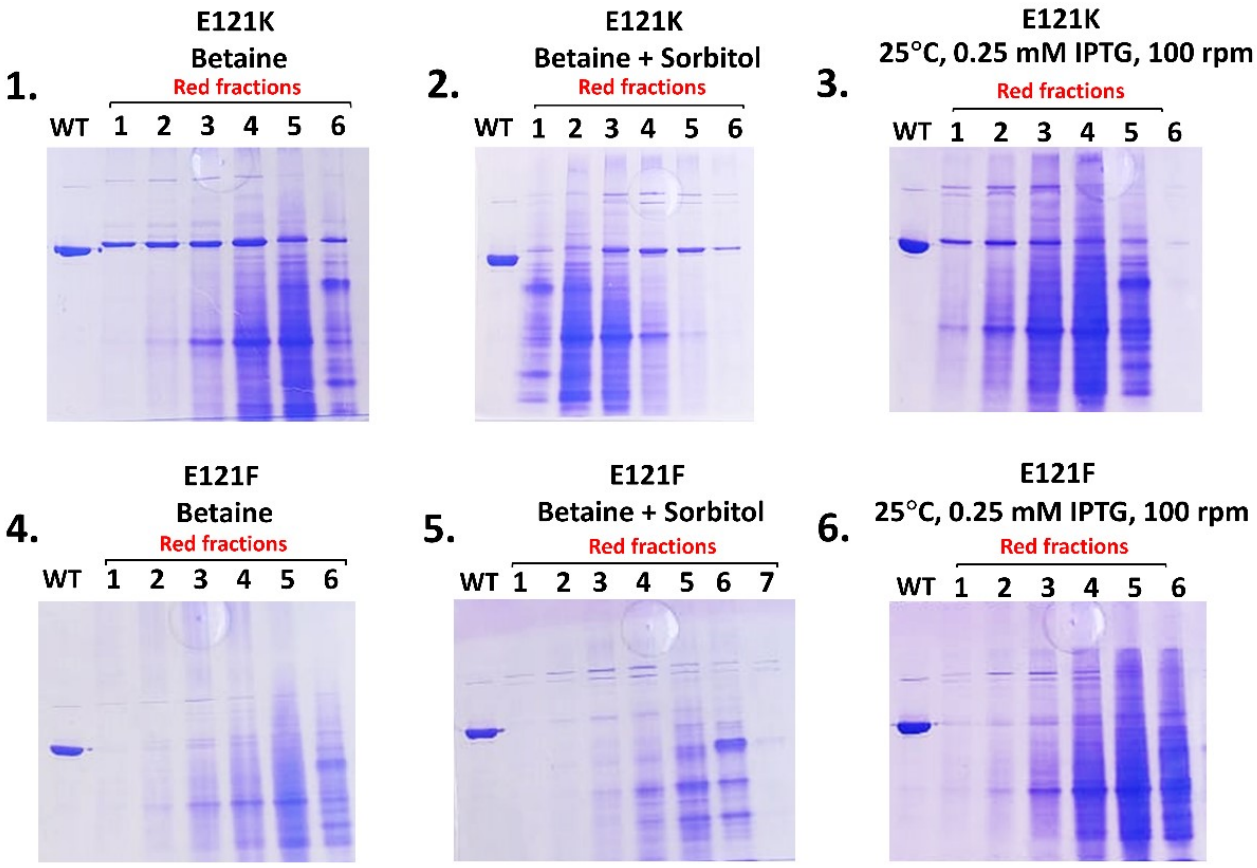

Figure S3: Native-PAGE (6%) profile of the eluted fractions of assembly-defective variants under modified over-expression conditions. The E121K variant exhibited partial, but improved, cage-assembly, as indicated by the presence of characteristic gel bands corresponding to cage species, whereas the E121F variant lacked such features. Details of the specific conditions are provided in the accompanying **Table S2**.

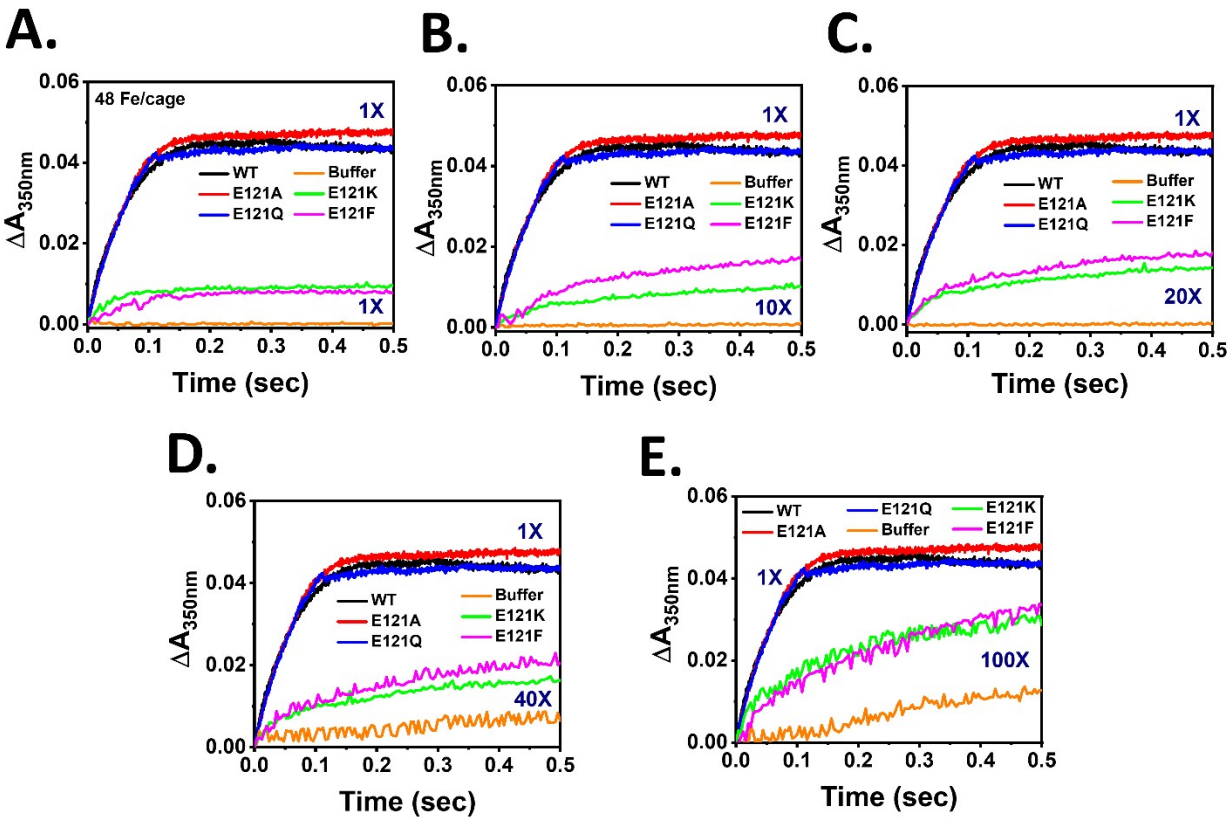

Figure S4. Comparison of rapid ferroxidase activity between self-assembled variants (~ 48 Fe/cage, 1X) and assembly-defective variants (~ 48 - 4800 Fe/cage, 1X - 100X). Progress curves of rapid ferroxidase activity of WT BfrA and its variants for the formation of $[Fe^{3+}\text{-}O]_x$ species at 350 nm, obtained by a stopped-flow rapid mixing system. For WT and assembled variants, final Fe^{2+} concentration was maintained at 50 μM (48 Fe/cage) in all cases. The final concentrations of iron for the assembly-defective variants and buffer were varied from 50 μM (1X) to 5 mM (100X). Here, buffer indicates autoxidation of respective iron amounts in absence of protein in 100 mM MOPS (pH 7.0). Final protein concentration was kept as 1.04 μM cage or cage equivalent for all variants. The folds of increase in Fe^{2+} concentrations are mentioned in the respective figures (see **Methods**).

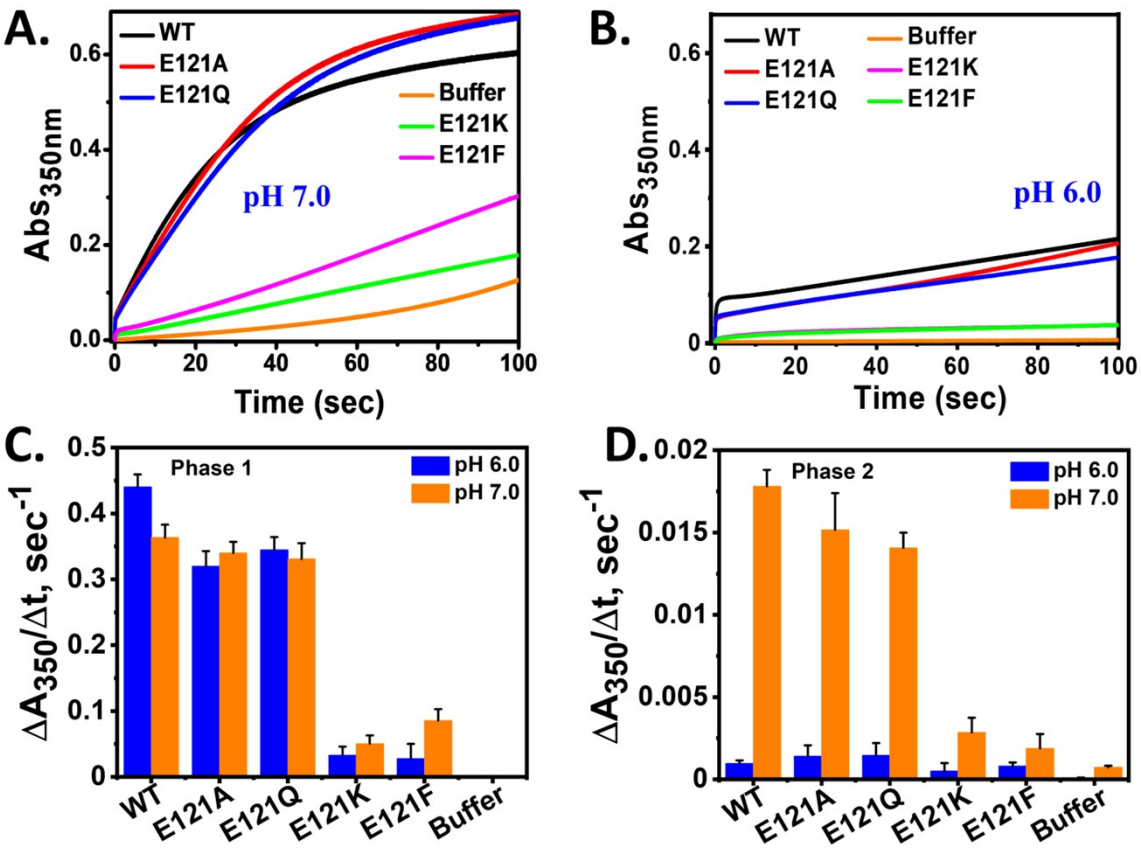

Figure S5. Impact of pH on the ferroxidase activity of E121 substituted *Mtb* BfrA variants monitored by stopped-flow rapid mixing spectrophotometer. Progress curves for the formation of $[Fe^{3+}\text{-}O]_x$ species at 350 nm for multiple-turnover (i.e., 480 Fe/cage) carried out in (**A**) 100 mM MOPS (pH 7.0) and (**B**) 100 mM MES (pH 6.0) and their respective initial rates of formation calculated from the linear fitting of the initial data points upto 120 ms and 5 secs respectively for **C.** Rapid phase and **D.** slow phase. Equal volume of 4.16 µM cage or cage equivalent of ferritin in respective buffers were mixed with 2 mM freshly prepared $FeSO_4$ solution) in a stopped-flow rapid mixing spectrophotometer to achieve 480 Fe/cage at 25 °C. Buffer represents autoxidation of iron in absence of protein (see **Methods**). For phase 1, p value for pH 6.0: ~ 0.035 and < 0.001 and p value for pH 7.0: > 0.05 and < 0.0001 for the assembled variants and assembly-defective variants (E121K and E121F) respectively, calculated with respect to WT. For phase 2, p value for pH 7.0: ~ 0.03 and < 0.001 for the assembled variants and assembly-defective variants (E121K and E121F) respectively, and p value for pH 6.0: > 0.05 for all the variants computed with respect to WT. The averages are of results of at least three independent experiments, using two different protein batches.

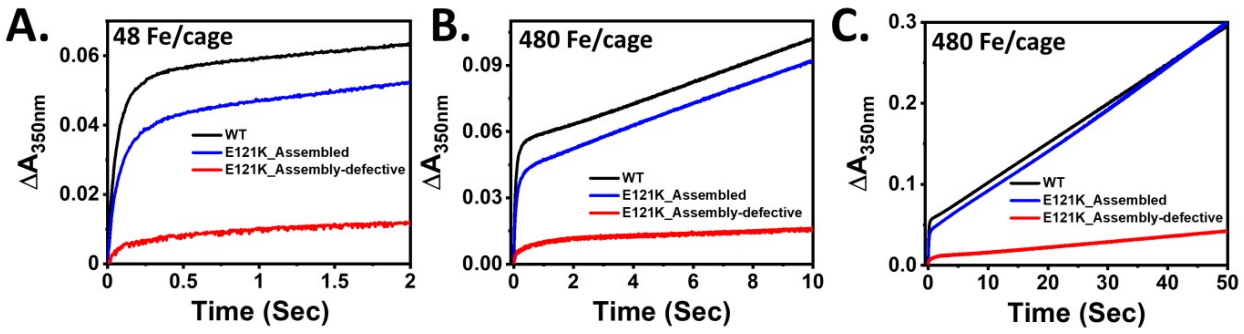

Fig S6: Comparison of ferroxidase activity of assembly-defective and assembled E121K variant. Progress curves for the formation of $[Fe^{3+}\text{-}O]_x$ species at 350 nm were monitored for WT and the assembled and assembly-defective forms of the E121K variant. Equal volumes of 1.04 μM cage or cage-equivalent protein solutions in 100 mM MOPS (pH 7.0) were mixed with freshly prepared $FeSO_4$ solution (in 1 mM HCl) using a stopped-flow rapid mixing spectrophotometer. Measurements were performed at Fe/cage ratios of **A.** 48 and **B**, **C.** 480, with Fig. **C** showing data recorded for 480 Fe/cage over a longer time scale.

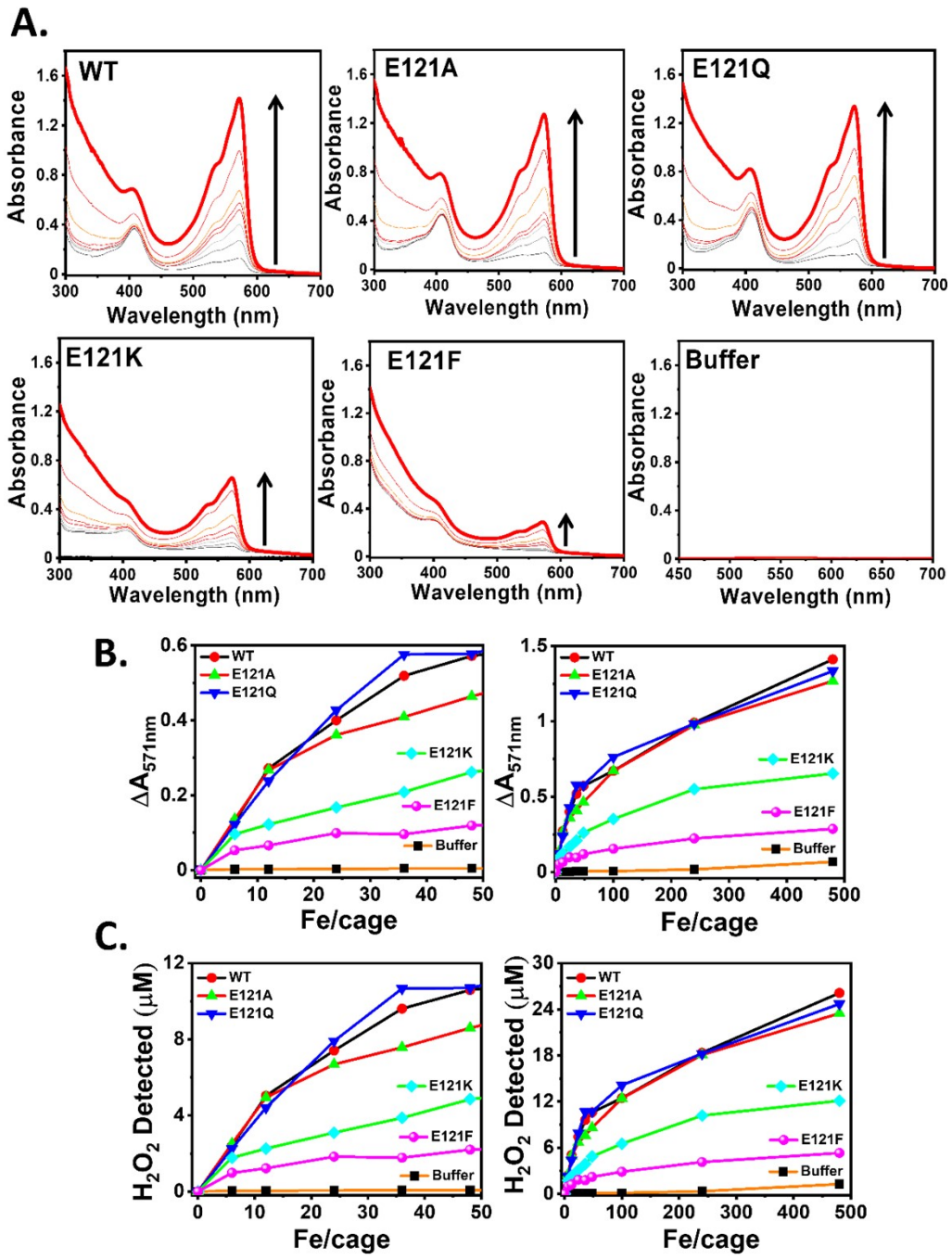

Figure S7. Detection of in situ generated H_2O_2 during ferroxidase/mineralization activity of *Mtb* BfrA variants. Absorption spectra recorded after ~3 min of addition of varying amounts of $FeSO_4$ solutions (0 – 480 μM) to a reaction mixture containing 50 μM of Amplex red, 0.5 μM of HRP and 1.04 μM cage/cage equivalent of protein solutions in 100 mM MOPS (pH 7.0) (**A**). The change in absorbance at 571 nm (ΔA_{571nm}), characterstic for the formation of resorufin (**B**) and amount of H_2O_2 detected (**C**) at different Fe/cage (0 – 48 and 0 – 480) for all the variants.

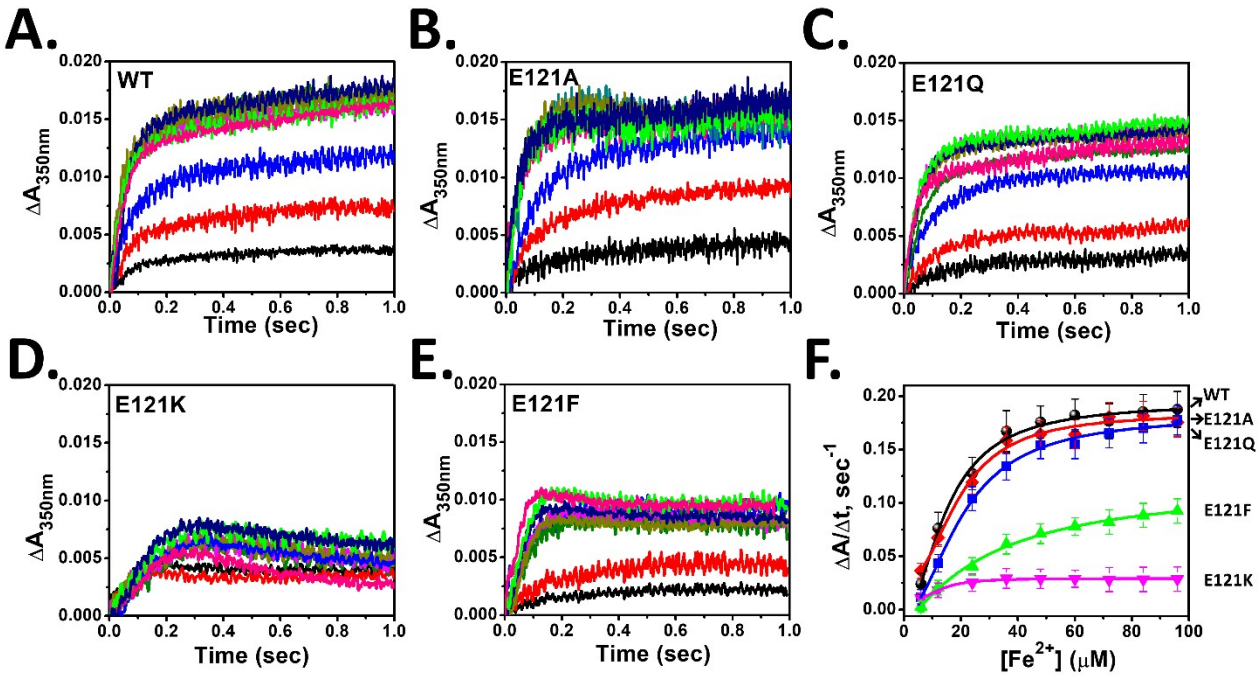

Figure S8. Titration of WT BfrA and its variants with increasing Fe^{2+} concentration. Progress curves for the formation of $[Fe^{3+}\text{-}O]_x$ species at 350 nm with increasing iron concentration in WT BfrA and its variants (**A-E**). The experiment was carried out in a stopped-flow spectrophotometer by equal mixing 2.08 μM (cage or cage equivalent) of protein solution with varying amounts of $FeSO_4$ solutions to achieve 6-96 Fe/cage. The initial rates for the formation of $[Fe^{3+}\text{-}O]_x$ species were obtained from the linear fitting of the data points (up to ~ 0.03 sec) and were plotted against iron concentration (**F**). The line represents the fitting of the initial rates with Hill equation (see **Methods**). Apparent kinetic parameters are presented in **Table S3**.

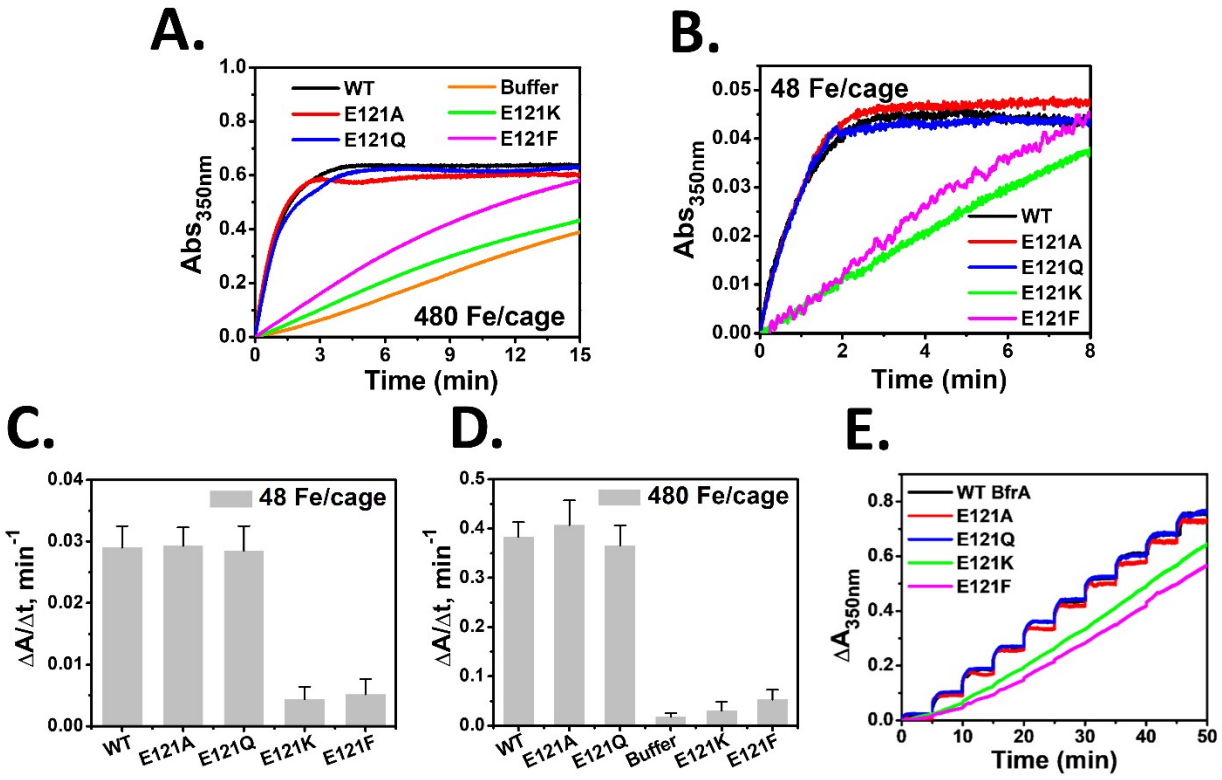

Figure S9. Iron oxidation/mineralization kinetics of WT BfrA and its variants by manual mixing. The iron mineralization process was monitored over longer time scale, using a UV-visible spectrophotometer, after manually adding freshly prepared $FeSO_4$ solution to 1.04 μM of WT BfrA and its variants in 100 mM MOPS buffer (pH 7.0) to achieve 48 (**A**) and 480 Fe/cage (**B**). The corresponding initial rates of iron oxidation/mineralization were calculated from the linear fitting of the data points (from panel '**A**' and '**B**') within ~ 1 min of data acquisition represented in '**C**' and '**D**'. The error bars signify the standard deviation obtained from the averages of three independent experiments using two different protein preparations. Sequential iron oxidation in WT *Mtb* BfrA and its variants was studied by monitoring the changes in A_{350nm} with ten subsequent additions of 48 Fe/cage, manually, to 1.04 μM ferritin protein solution in 100 mM MOPS buffer (pH 7.0) (**E**) (see **Methods**). For $[Fe^{3+}\text{-}O]_x$ species at 350 nm, p value > 0.05 and < 0.0001 for the assembled variants and assembly-defective variants (E121K and E121F) respectively, calculated with respect to WT. The averages are of results of at least three independent experiments, using two different protein batches.

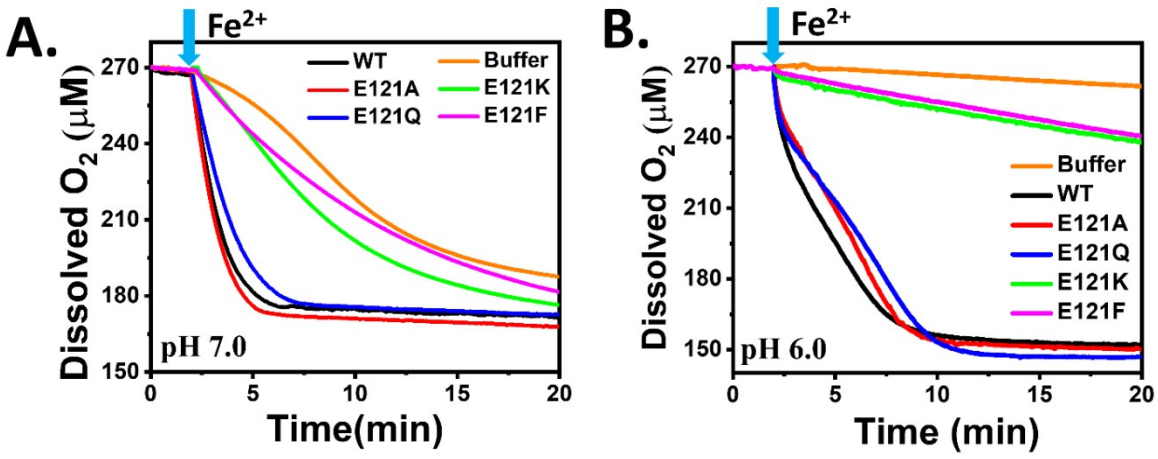

Figure S10. pH dependent O_2 consumption kinetics during the ferroxidase/mineralization activity of self-assembled and assembly-defective *Mtb* BfrA variants. Freshly prepared $FeSO_4$ solutions (240 μM) were added to 0.5 μM protein cage in **A.** 100mM MOPS, pH 7.0 and **B.** 100mM MES, pH 6.0 using a Hamilton syringe to achieve 480 Fe/cage. Arrow indicates the time point of Fe^{2+} addition.

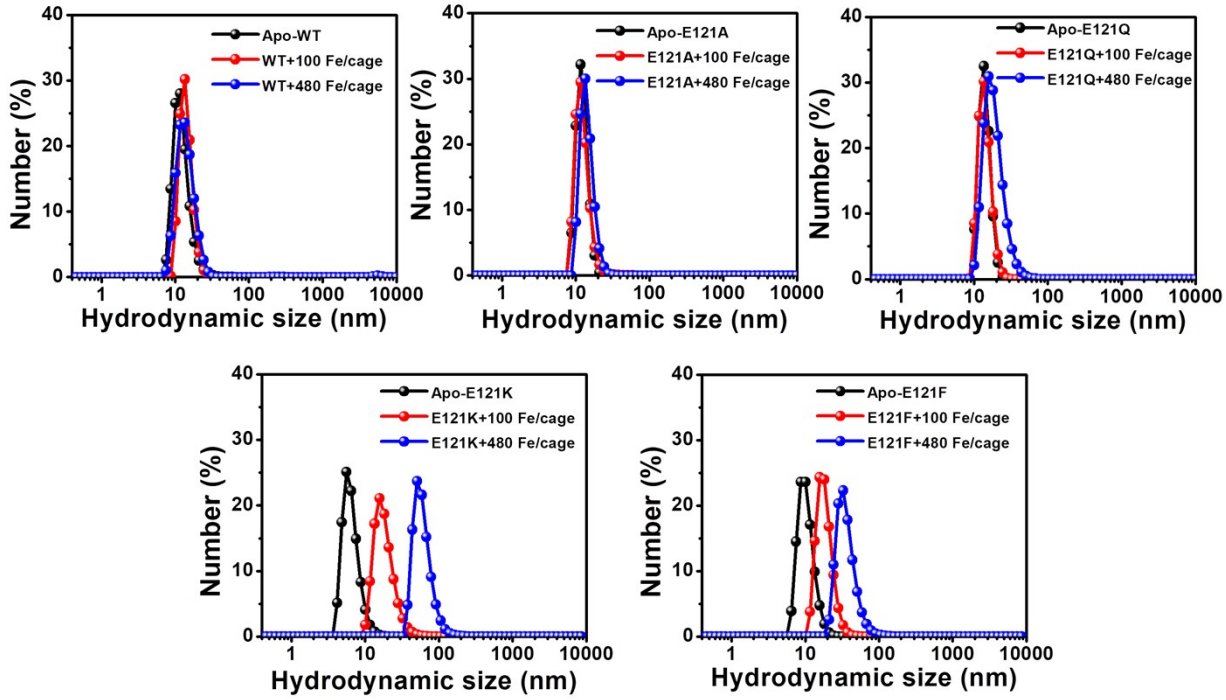

Figure S11. Dynamic light scattering measurements of apo- and Fe^{2+} mineralized samples of WT BfrA and its variants. The experiment was performed with 1.04 μM cage or cage equivalent of protein solution in 100 mM MOPS (pH 7.0), before and after addition of 100 (4 Fe/subunit) and 480 (20 Fe/subunit) Fe/cage. The experiment was carried out at 25 °C. Hydrodynamic sizes are listed in Table S3.

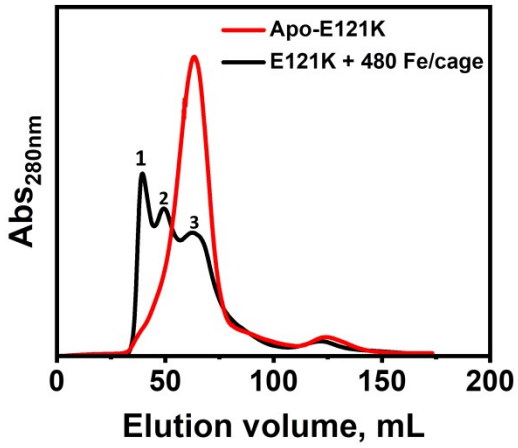

Figure S12: Size-exclusion chromatogram (SEC) profile of soluble fraction mineralized E121K. The absorbance profile shows three distinct fractions (**1**, **2** and **3**), with the third fraction coinciding with the apo-protein profile. The additional fractions **1** and **2** possibly correspond to some relatively larger sized species such as: soluble Fe^{3+} aggregates (iron-oxide clusters) on the

surface of the protein and/or iron-induced higher order oligomeric assemblies including a small fraction of cage like structure (as observed at 5x higher protein concentrations in **Fig 2B** of the original manuscript).

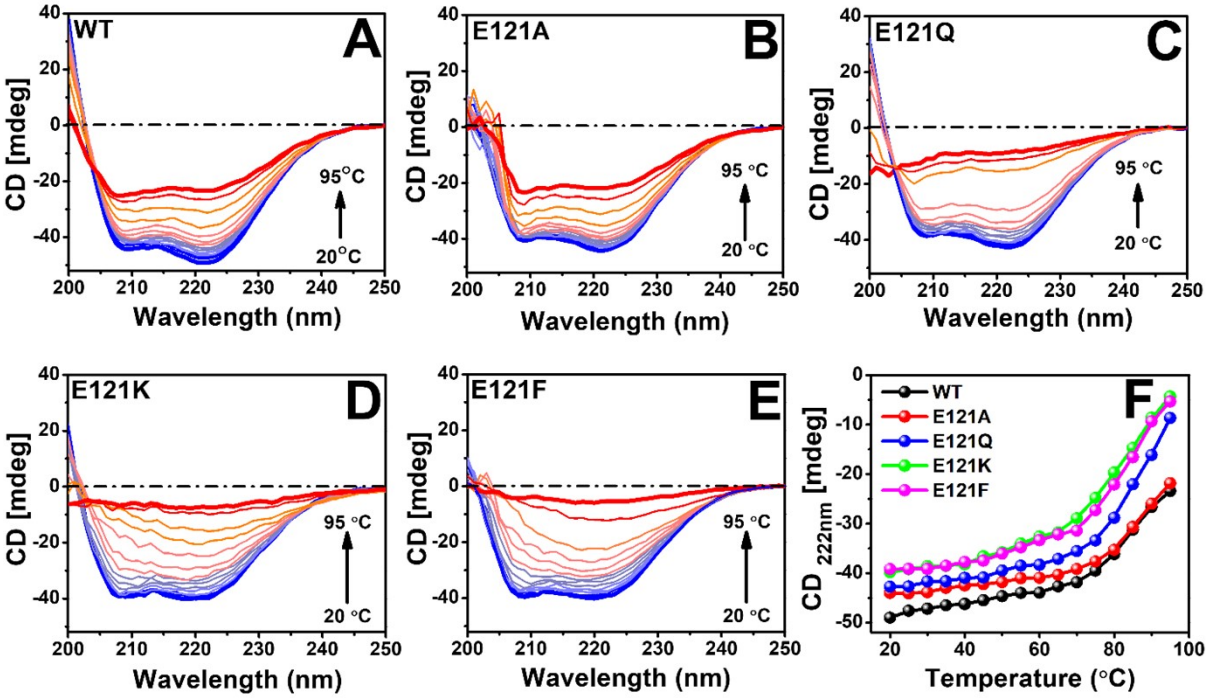

Figure S13. Temperature induced unfolding of self-assembled and assembly-defective *Mtb* BfrA variants. Far-UV CD spectra of WT BfrA and its variants were recorded by increasing the temperature from 20–95 °C in a Jasco J-1500 CD spectrometer (**A**-**E**). Changes in the CD signal at 222 nm with varying temperature (**F**). Protein concentration was maintained at 0.25 µM cage or cage equivalent (6 µM subunit).

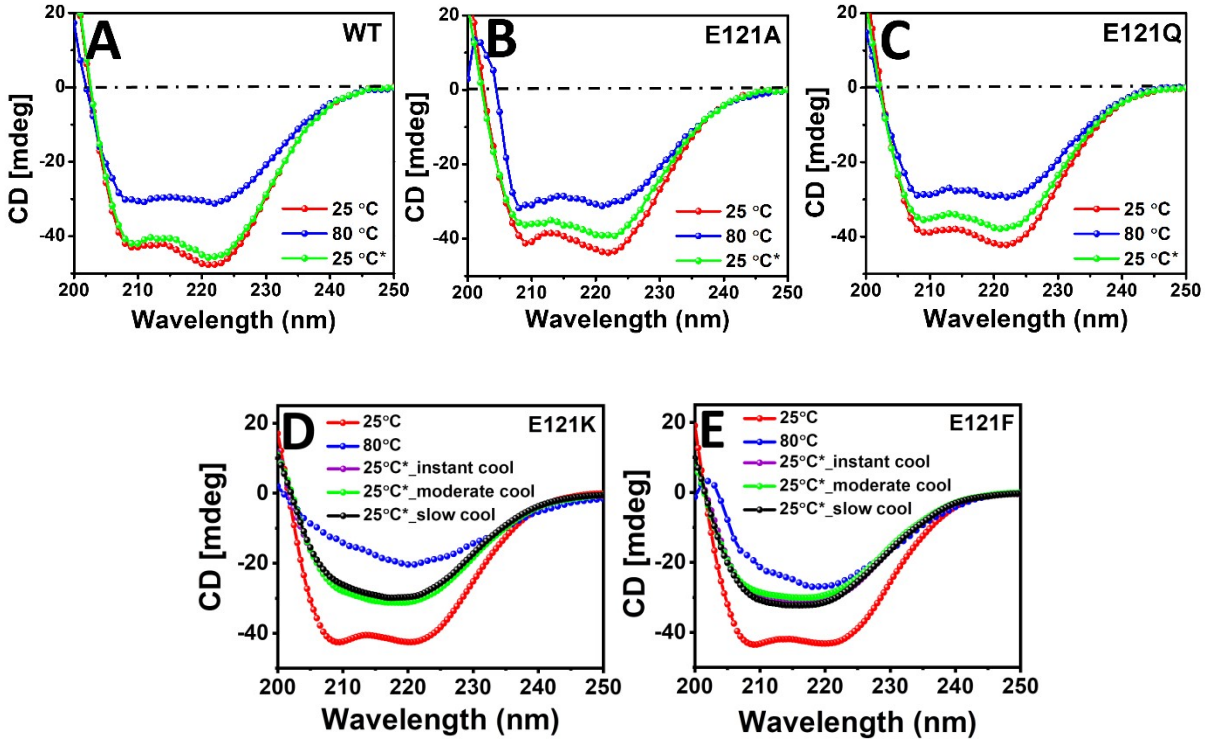

Figure S14. Far-UV CD spectra of self-assembled and assembly-defective *Mtb* BfrA variants. The 25 °C* traces were recorded after cooling back the samples from 80 to 25 °C. For the E121K and E121F variants, 25 °C* traces were recorded after cooling back the samples from 80 to 25 °C, under three conditions: (1). instant cooling by immersing the sample tube in water (~ 6 mins) (2). moderate cooling at room temperature (~ 21 mins) and (3). slow controlled cooling in a dry bath (~ 1 hour 20 mins). The assembly-defective variants exhibited irreversible unfolding under all conditions as opposed to WT and self-assembled variants (E121A, E121Q), which exhibited reversible unfolding.

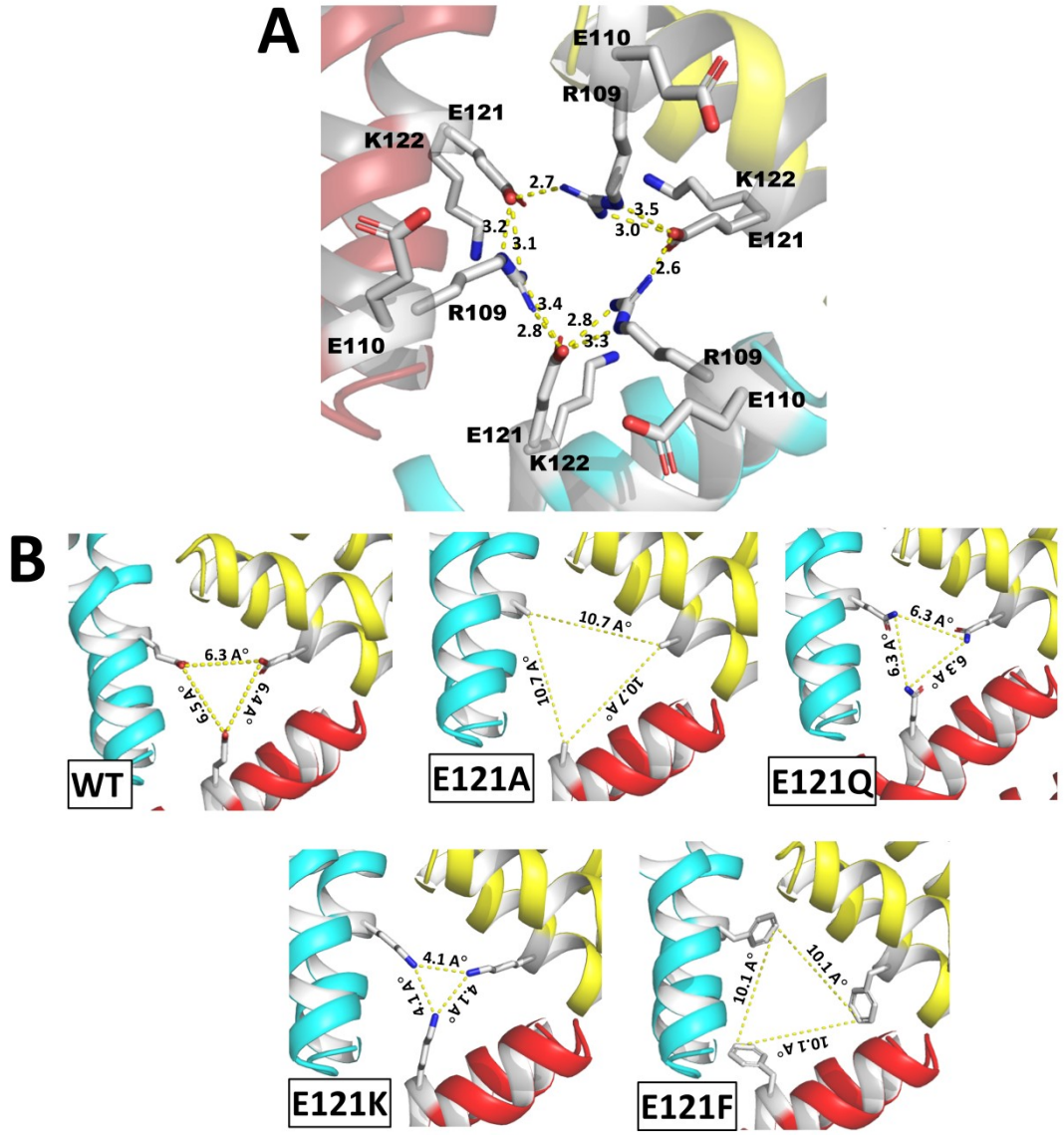

Figure S15: A. Representation of the inter-subunit interactions between the E121 and R109 residues at the 3-fold pore of WT *Mtb* BfrA. Labelled distances are in Å units. **B.** Inter-subunit distances between 121th residue of the three subunits at the 3-fold pore. The calculations reveal that the distance between E121 and E121 is ~6.4 Å (in WT), whereas F121 and F121 (E121F) is 10.1 Å; with a noteworthy reorientation of K122 (WT: E121 – K122 ~ 12.5 Å; E121F: F121 – K122 ~ 6.6 Å) (**Table S6**). These values further corroborate the impact of Phe in imparting steric obstruction during self-assembly process in E121F. The unusually greater pore distance in E121A is owing to the shorter side chain of alanine. Structures are obtained using Alpha Fold 3.0[1].

RAW DATA FOR FIGURE – 2 and 5

Figure 2A: SDS-PAGE

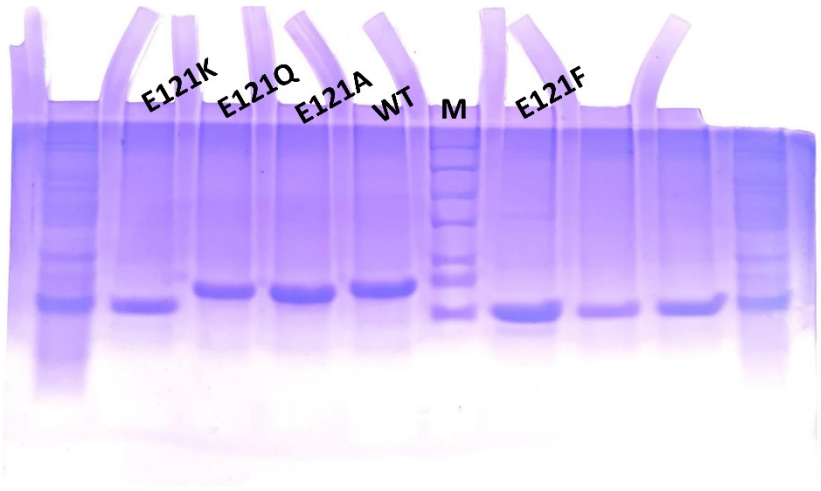

Figure 2B: Native-PAGE - Prussian (Iron) Staining

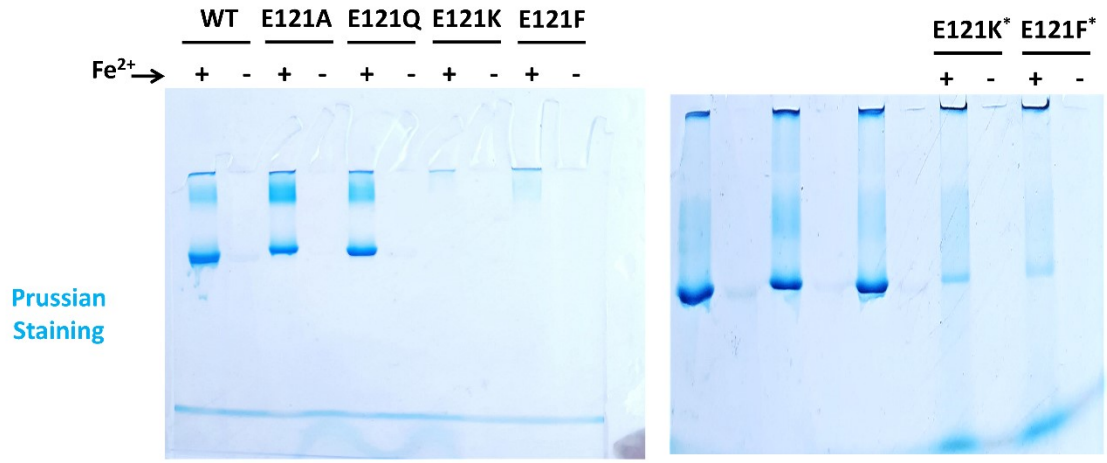

Figure 2B: Native-PAGE – Coomassie (Protein) Staining

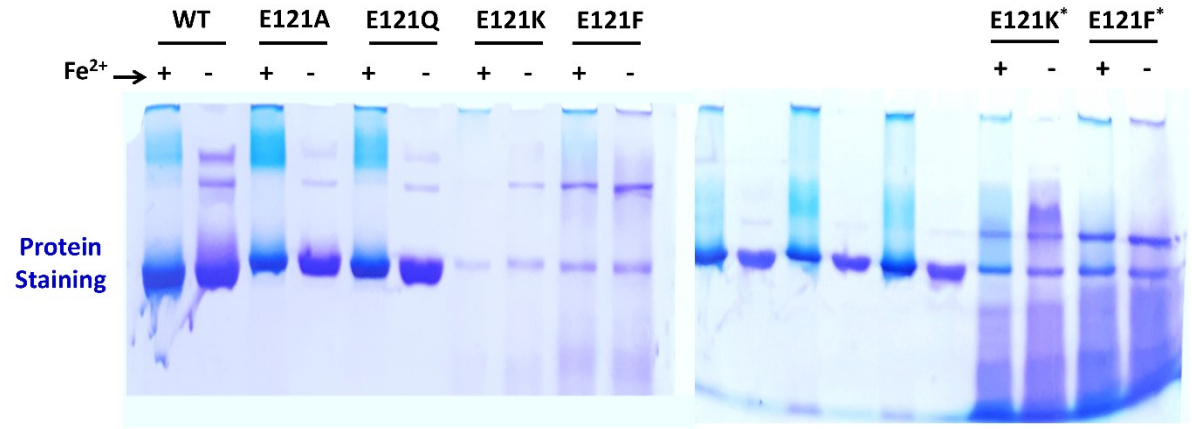

Figure 5B: Native-PAGE - Prussian (Iron) and Coomassie (Protein) Staining

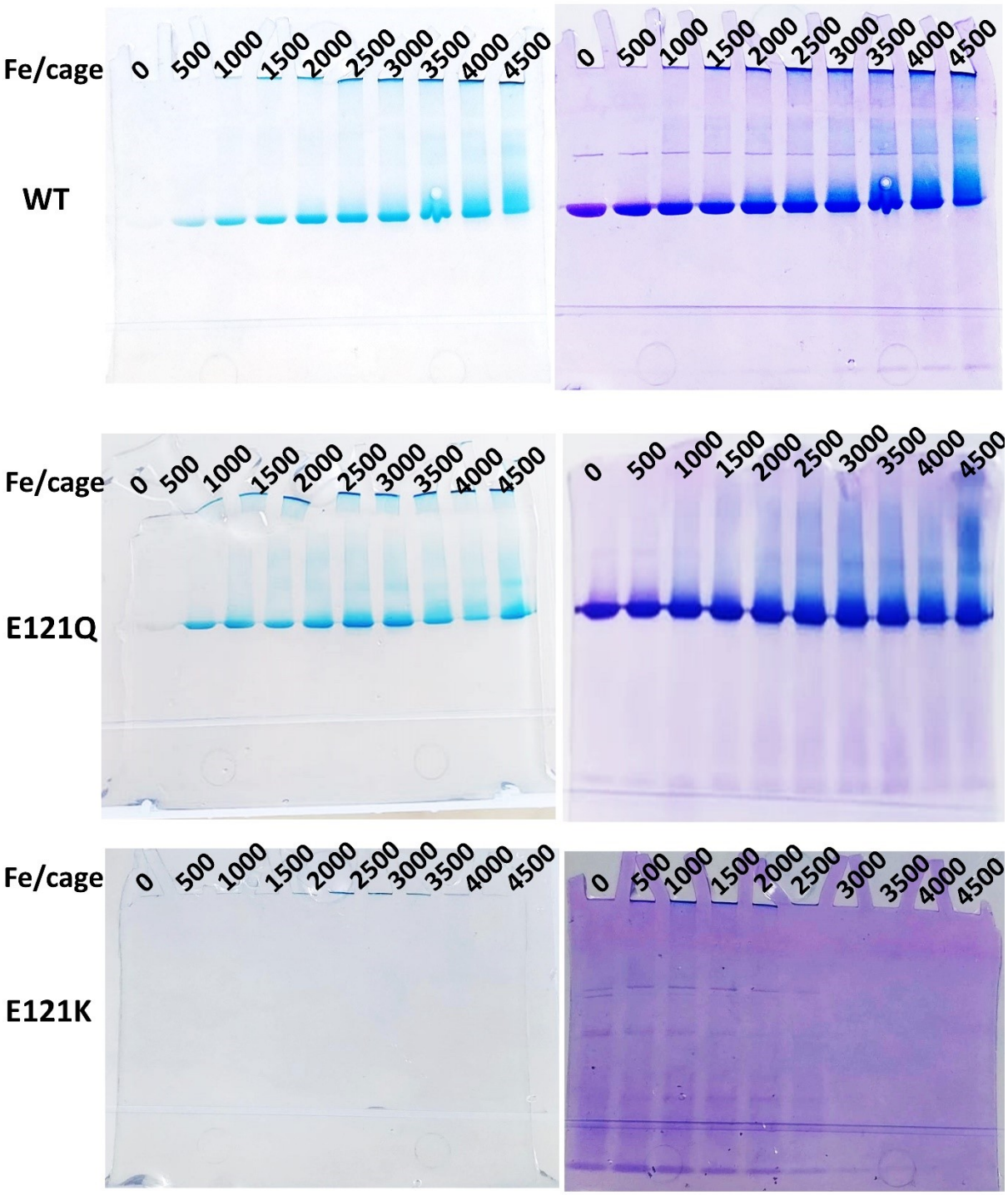

Figure 5C: Agarose gel

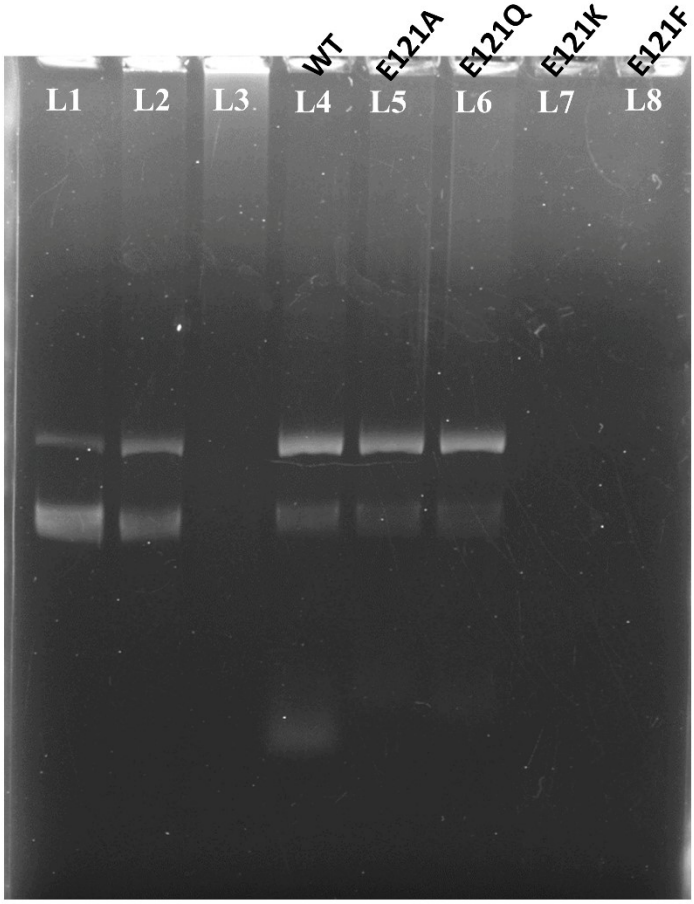

DNA	+	+	+	+	+	+	+	+
$FeSO_4$	-	+	+	+	+	+	+	+
H_2O_2	-	-	+	+	+	+	+	+

Figure S3: Native-PAGE – Coomassie (Protein) Staining

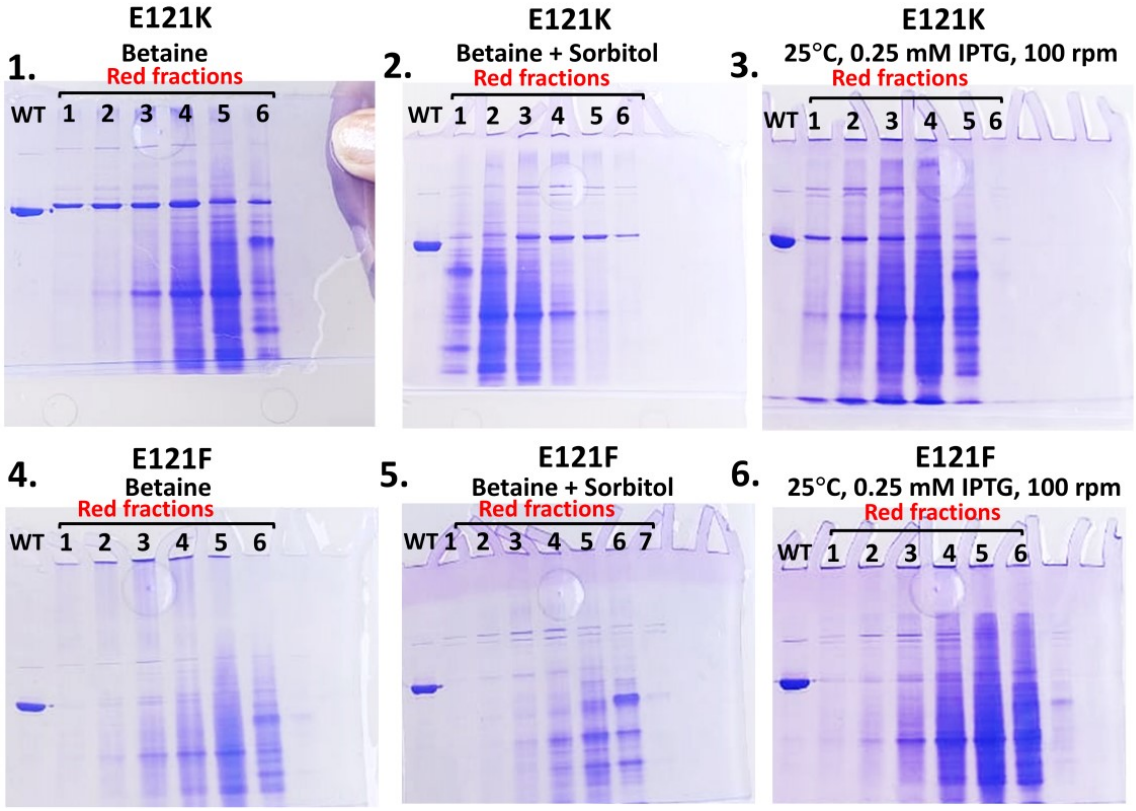

References

1. Abramson, J et al. Accurate structure prediction of biomolecular interactions with AlphaFold 3. Nature (2024).